METEOROLOGICAL FACTORS IN EARTH-SATELLITE PROPAGATION

C.A. Levis
R.C. Taylor
R. Leonard
K.T. Lin
B. Pigon
A. Weller

The Ohio State University

ElectroScience Laboratory

Department of Electrical Engineering
Columbus, Ohio 43212

Annual Report 713656-2

March 12, 1981 - March 31, 1982

Jet Propulsion Laboratory
California Institute of Technology
Pasadena, California 91103

NOTICES

When Government drawings, specifications, or other data are used for any purpose other than in connection with a definitely related Government procurement operation, the United States Government thereby incurs no responsibility nor any obligation whatsoever, and the fact that the Government may have formulated, furnished, or in any way supplied the said drawings, specifications, or other data, is not to be regarded by implication or otherwise as in any manner licensing the holder or any other person or corporation, or conveying any rights or permission to manufacture, use, or sell any patented invention that may in any way be related thereto.

50272-101

REPORT DOCUMENTATION PAGE	1. REPORT NO.	2.	3. Recipient's Accession No.

4. Title and Subtitle

METEOROLOGICAL FACTORS IN EARTH-SPACE PROPAGATION

5. Report Date
March 1982

6.

7. Author(s)
C.A. Levis, R.C. Taylor, et al.

8. Performing Organization Rept. No
ESL 713565-2

9. Performing Organization Name and Address

The Ohio State University ElectroScience Laboratory
Department of Electrical Engineering
Columbus, Ohio 43212

10. Project/Task/Work Unit No.

11. Contract(C) or Grant(G) No
(C) 956013
(G)

12. Sponsoring Organization Name and Address

Jet Propulsion Laboratory
California Institute of Technology
Pasadena, California 91103

13. Type of Report & Period Covered
Annual Report
3/12/81 - 3/31/82

14.

15. Supplementary Notes

16. Abstract (Limit: 200 words)

Using the COMSTAR D/4 28.56 GHz beacon as a source, a differential gain experiment was performed by connecting a 5-meter paraboloidal antenna and a 0.6-meter paraboloidal antenna alternately to the same receiver. Substantial differential gain changes were observed during some, but not all, rain events.

A site-diversity experiment has been implemented; it consists of two 28.56 GHz radiometers separated by 9 km. The look-angle corresponds to that of the D/4 beacon, and data was obtained with one radiometer during several weeks of concurrent beacon operation to verify the system calibration. A theoretical study of the effect of scattering from a non-uniform rain distribution along the path is under way to aid in interpreting the results of this experiment.

An improved empirical site diversity-gain model has been derived from data in the literature relating to 34 diversity experiments.

Work on the experiment control and data acquisition system is continuing with a view toward future experiments.

17. Document Analysis a. Descriptors

Propagation
Satellite Communications
Rain Effects

b. Identifiers/Open-Ended Terms

Diversity
Gain
Antenna/medium coupling
Radiometer

c. COSATI Field/Group

18. Availability Statement	19. Security Class (This Report)	21. No. of Pages
	Unclassified	51
	20. Security Class (This Page) Unclassified	22. Price

(See ANSI-Z39.18) See Instructions on Reverse OPTIONAL FORM 272 (4-7
(Formerly NTIS-35)
Department of Commerce

TABLE OF CONTENTS

LIST OF TABLES

LIST OF FIGURES

I. INTRODUCTION

This contract has been concerned with the degradation of communication satellite signals at 28.56 GHz by rain and clouds. The following tasks were performed.

One proposed method of overcoming the attenuation due to rain is to use antennas with more gain and therefore larger apertures. A possible difficulty with this approach is that the gain of large antennas may not be fully realized during rain periods due to perturbation of the phase front arriving at the antenna by scattering from the hydrometeors. One task therefore consisted of measuring the degradation of the gain of an antenna having a diameter of 5 meters. The signal source for this experiment was the Comstar D/4 geo-synchronous satellite beacon at 28.56 GHz. This beacon became available on 11 March 1981 and ceased operation on 1 September 1981.

A second proposed method of overcoming rain attenuation is by site-diversity; i.e., by suitably choosing among (or combining) the signals received at two or more sites. The sites must be sufficiently close to allow a terrestrial link to transmit the received signal between them while being sufficiently distant from each other to make the likelihood of simultaneous deep fades sufficiently small. The brief operational period of the Comstar D/4 beacon at 28.56 GHz made it impossible to gather sufficient rain attenuation statistics with this source alone. Therefore, two radiometers were activated at 28.56 GHz and pointed in the same direction, which coincides with that to the D/4 beacon. The rain attenuation can be inferred, within limits, from such radiometric

measurements. The method of inferring attenuation from radiometric temperature has, however, some ambiguities; it was therefore considered important to obtain some simultaneous radiometric and beacon signal transmission measurements in order to validate the conversion. The implementation of the diversity-radiometer system constituted the second task under this contract.

The concept of path (site) diversity is not new and experiments addressing it have been made at a variety of frequencies and locations. An empirical model for interpreting these measurements and predicting the performance of proposed systems had been formulated earlier on the basis of the then existing data base. More data has become available since that initial formulation; a third task under the contract consisted of improving the path-diversity model by utilizing the currently available data base.

Some alternative tasks were specified in the contract, to be performed in case the Comstar D/4 beacon should not become available during the contract period. One of these was the continuation of operation of an S-band radar which had been used to generate rain-rate information along the earth-satellite path under a program sponsored by the International Satellite Communications Organization. Rain-rate data along the path can be enormously useful for interpreting attenuation and radiometric measurements. Therefore, although the condition of beacon unavailability did not apply, it was decided to continue operation of the radar on a low-priority basis, i.e., for rain events occurring during normal working hours and for which the presence of an operator

would not lead to neglect of more important tasks or to significant expense.

These explicitly specified tasks imply also two additional problems to be addressed. First, an assessment needs to be made on how well radiometric measurements at this frequency predict attenuation measurements, considering specifically the fact that scattering as well as absorption is a significant extinction mechanism at this frequency. It turns out that the distribution of rain along the path appears to be of some importance in relating the two measurements; this was an additional reason for maintaining limited operation of the S-band radar. A theoretical study relating the radiometric and signal transmission experiments has been undertaken to determine the best way of interpreting radiometric measurements in terms of attenuation. Second, under a concurrent program sponsored by the International Satellite Communications Organization, comparisons are being made between radar-inferred, radiometrically inferred, and directly measured signal attenuation on the basis of experimental data. Since the direct attenuation experiment was performed under this contract, it has been agreed that the final results under the Intelstat program will also be made available under this contract.

II. THE GAIN-DEGRADATION EXPERIMENT

A. Implementation

The gain-degradation experiment consists in switching a receiver periodically between two antennas mounted on the same axis. The first

is a 5-meter (diameter) Cassegrainian paraboloid which might be expected potentially to exhibit gain changes; the second is a focal-point-fed 0.6-meter (diameter) paraboloid mounted in front of the Cassegrain sub-reflector, which should experience little gain change because of its small size. The system is shown schematically in Figure 1; a photograph of the antennas appears in Figure 2; and the system block diagram is shown in Figure 3. The entire receiver chain from the switch on is common to both antennas, so that the comparison of signal levels is insensitive to receiver gain changes. The gain-degradation experiment had been designed originally for use with the Comstar D/3 beacon, but had to be converted to 19.04 GHz when the 28.56 GHz beacon on that satellite became unavailable. The reconversion to 28.56 GHz was accomplished just prior to the beginning of this contract. Concurrently with the gain degradation measurements, simultaneous measurements of radar backscatter at 3 GHz and radiometric temperature at 8.5 GHz were made along the same propagation path. The radar backscatter was recorded in 100 range bins, each 150m long, thus obtaining a profile of the reflectivity factor along the propagation path. A calibrated rain tipping bucket was in operation at the site location. During the period from March 11, 1981 to September 1, 1981 over 75 rain and thunderstorm events were recorded.

B. Data Acquisition and Calibration

Two data channels were used in the experiment. One is the receiver output and the other is the switch drive signal; these two channels along with radar, radiometer, and station-keeping data were recorded on

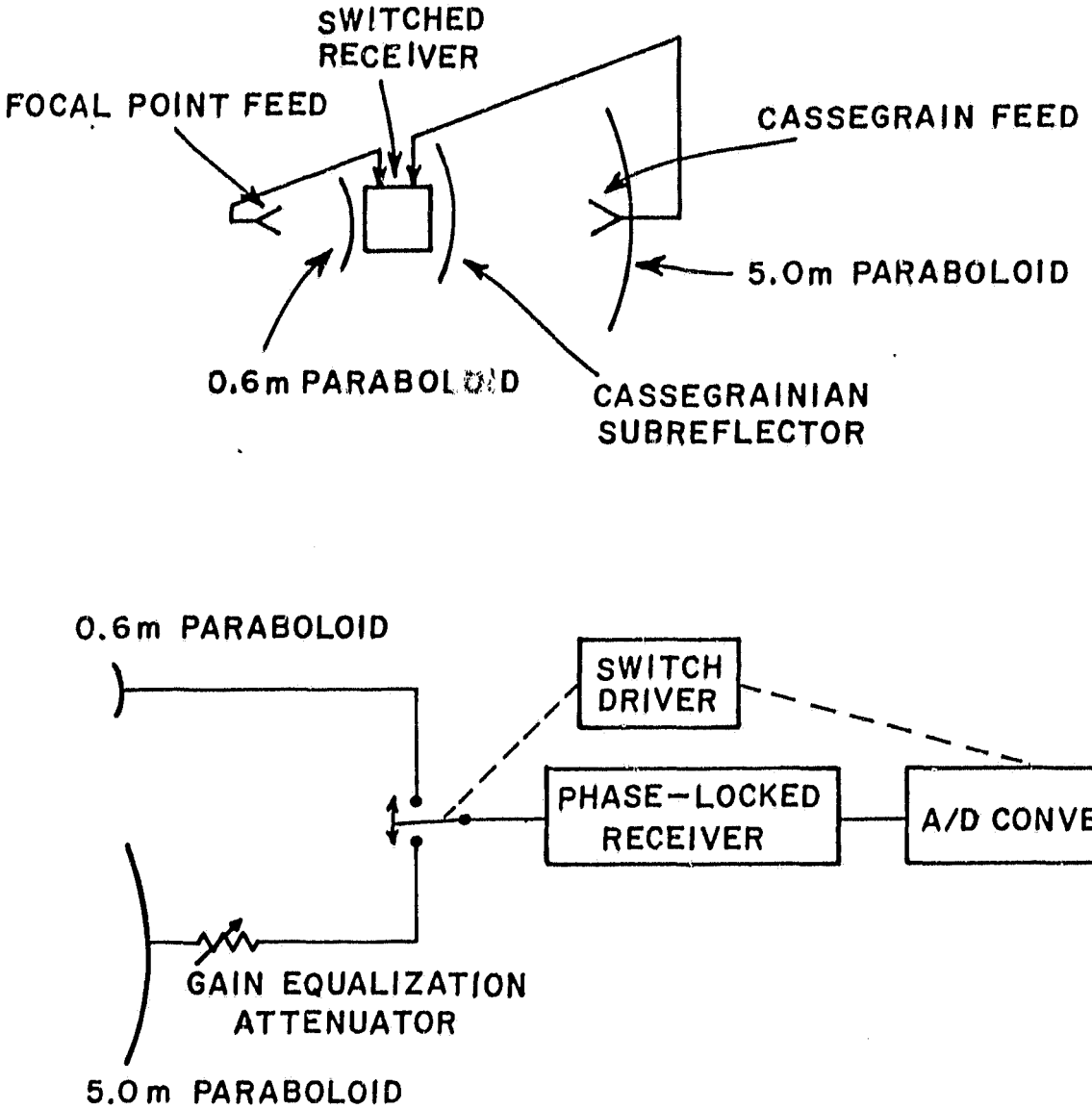

Figure 1. Gain-degradation experiment concept.

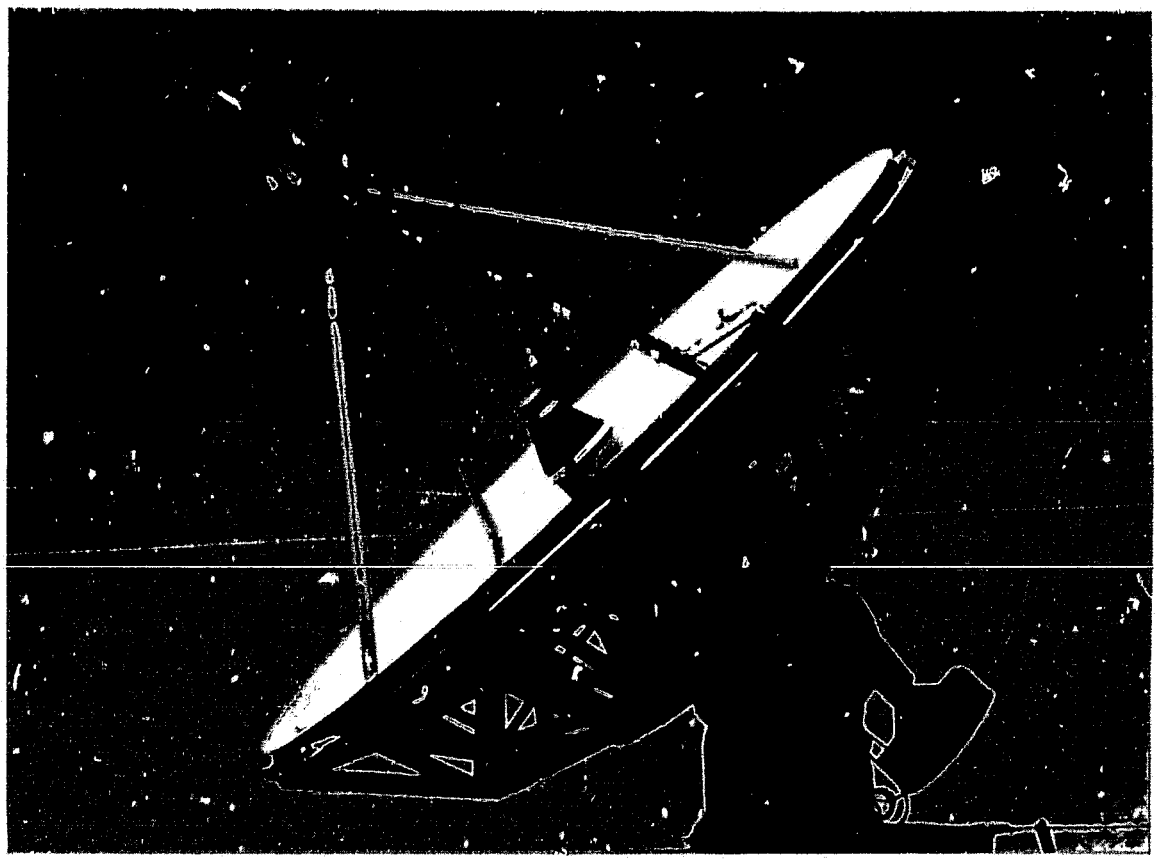

Figure 2. Gain-degradation experiment antennas.

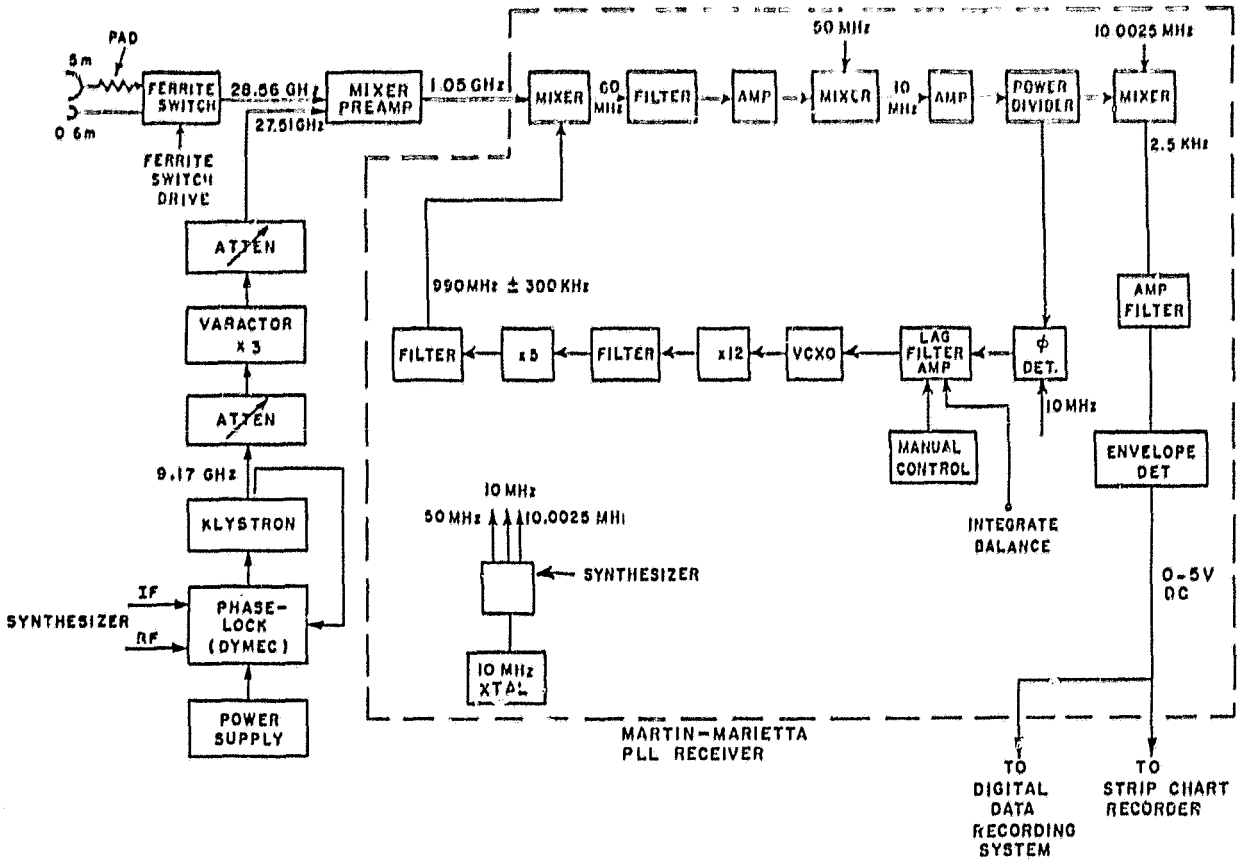

Figure 3. Gain-degradation experiment block diagram.

9-track magnetic tape. The record format, which has been used previously, is given in Table 1; the channels applicable here are numbers 14 and 15 and the record type is 13, i.e., sampling at 3-second intervals. Since the receiver was switched every thirty seconds between antennas, ten samples were obtained from each antenna before the switch transferred the receiver to the other antenna. The samples were digitized by an 8-bit converter capable of measuring from -5 to +5 volts in 256 levels. Since the receiver output ranged from 0-5 volts, a useful output of 128 levels was obtained. The ferrite switch drive signal was also sampled and digitized, so that each received signal sample could be associated with the proper antenna. The switch signal had levels of 0 and 5 volts; a 5-volt level means that the 5-m antenna was selected.

A calibration is needed to convert the output voltages into input signal power levels. Since only the relative received signal power levels are of interest in this experiment, the receiver is calibrated with respect to an arbitrary level somewhat above the maximum signal output level. In order to calibrate the entire system, a signal source was placed in the field approximately 150 feet in front of the antennas. The 28.56 GHz source was obtained from a highly stable 9.52 GHz signal generator, frequency-multiplied by 3, and attenuated by a high-precision attenuator. The input signal was varied with the attenuator from 0 to -32 dB in 1dB steps. Each attenuation level was held for 30 seconds and was sampled at 3 second intervals and recorded on digital tape in the usual signal format. The calibration curve, Figure 4, shows the receiver output level for a given input signal level, expressed as an

TABLE 1

RECORD TYPE 13 FORMAT

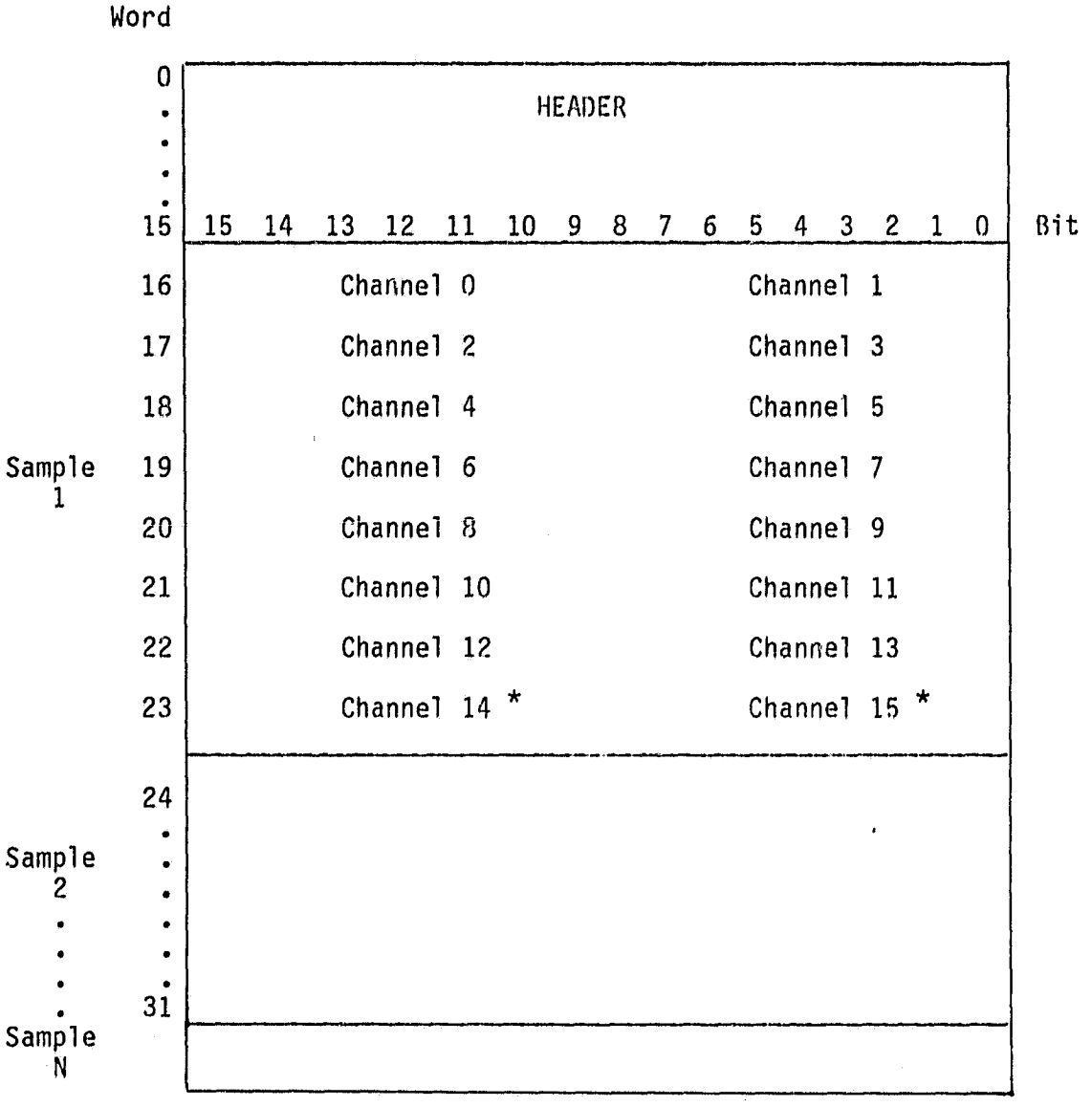

N_{max} = 32 (272 word record)
Corresponding to 96 seconds

*Channel 14: Gain-degradation experiment switch
*Channel 15: Gain-degradation experiment signal

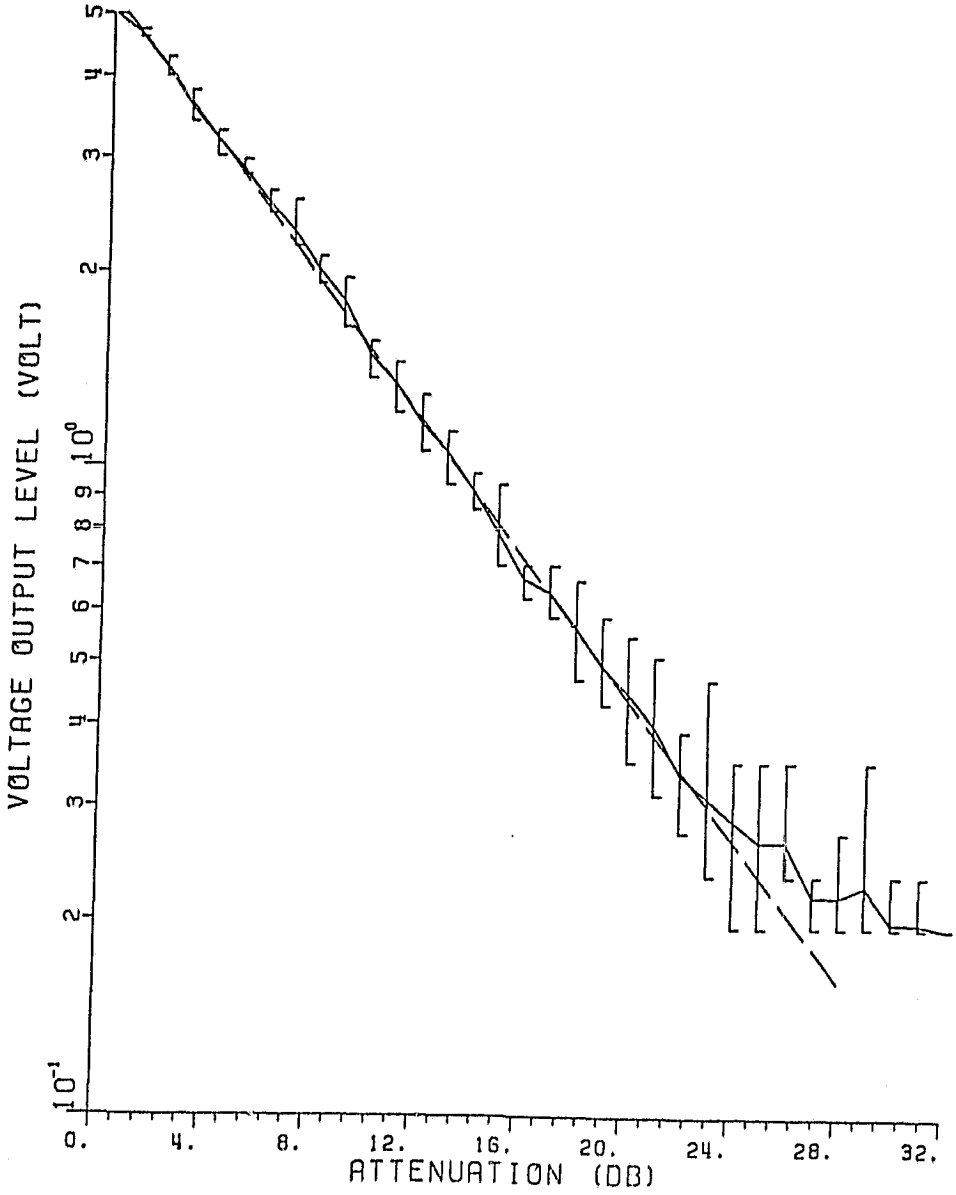

Figure 4. Gain-degradation experiment calibration.

attenuation below the selected reference level. Since the receiver detector is of square law, a plot of the logarithm of the output voltage against the input attenuation levels in dB is approximately linear. The dotted line in the figure is a linear-regression fit to the data; the brackets indicate the extremes. All the digitized received signals could then be expressed as the relative attenuation levels in decibels by means of the calibration curve. The system resolution is 0.063 dB at a signal level of 0 dB and 1.073 dB at a level of -22 dB.

C. Data Processing

In order to process the data efficiently, the original data tapes were first copied to a tape with a compressed tape format. Only the gain-degradation experiment data was copied; thus, 23 original data tapes were compressed into one tape. The data word length, originally 3 bytes, was reformatted to 4 bytes for processing by the VAX 11/780. This tape was used as input for a program to compute the signal means and variances as discussed below, the results being stored on a third tape.

The relative received power P(t) and amplitude A(t) are defined as

$$P(t) = \frac{p(t)}{p_o} = 10^{\frac{P_{dB}(t)}{10}} , \qquad (1)$$

$$A(t) = \frac{a(t)}{a_o} = 10^{\frac{P_{dB}(t)}{20}} , \qquad (2)$$

where $p(t)$ is the absolute power of the received signal, p_o is an arbitrary power level selected at the calibration period, and $P_{dB}(t)$ is the relative attenuation as determined from the receiver calibration characteristics. The quantities $a(t)$ and a_o are the amplitudes corresponding to $p(t)$ and p_o. Since we are only interested in the relative values, the choice of p_o is of no consequence.

The mean and variance of each signal was computed for every thirty-second time period. The variances are normalized to the mean power level of the signal over the same time period. They are given by

$$\bar{A} = \frac{1}{N} \sum_{i=1}^{N} A(t_i) \quad , \tag{3}$$

$$\sigma_{dB}^2 = 10 \log_{10} \sum_{i=1}^{N} \frac{(A(t_i)-\bar{A})^2}{N\bar{A}^2} \quad , \tag{4}$$

where $A(t_i)$ is the i-th sample of the relative received amplitude, and N was set equal to 10. The gain reduction R is defined to be

$$R = 10 \log_{10} \frac{\bar{A}_1^2(t)}{\bar{A}_{10}^2(t)} = 20 \log_{10} \bar{A}_1(t) - 20 \log_{10} \bar{A}_{10}(t) \quad , \tag{5}$$

where $\bar{A}_1(t)$ is the signal mean given by Equation (3) during a rain event, and $\bar{A}_{10}(t)$ is the relative signal mean if meteorological effects were absent, i.e., on a corresponding "clear" day. The gain difference ΔG between 0.6m and 5m antennas is defined to be,

$$\Delta G(t) = R_2(t) - R_1(t) \quad , \tag{6}$$

where $R_1(t)$ is the gain reduction of the 5-m antenna, and $R_2(t)$ is the gain reduction of the 0.6-m antenna.

Because of the diurnal motion of the satellite, the antenna axis did not always point precisely at the beacon source. This pointing error had only a small effect on the output of the small antenna due to its large (about 1°) beam width, but the signal received by the 5-m antenna varied slowly and smoothly with a period of about 24 hours. This effect was removed in the process of data analysis by using for $\overline{A}_{10}(t)$ a value from an adjacent "clear" day at the same point in the diurnal cycle; if the corresponding diurnal period on adjacent days did not have "clear" weather, the nearest "clear" day was used, with some loss of accuracy.

D. Results

Preliminary results for the experiment are shown in Figure 5. The first set of data in the figure, taken on day 151 (Julian date) is included primarily to show the effectiveness of removing the diurnal drift of the satellite with respect to the fixed antenna axis. This day occurred early in the experiment, while the receiving antenna axis was still being adjusted, and the antenna was not pointed very accurately as a consequence. The pointing error puts the satellite on the relatively strongly sloping part of the antenna pattern of the large dish, resulting in a mean gain change of about 5 dB over the 4-hour data period. The gain difference curve shows that this variation has been subtracted out to within approximately 0.3 dB.

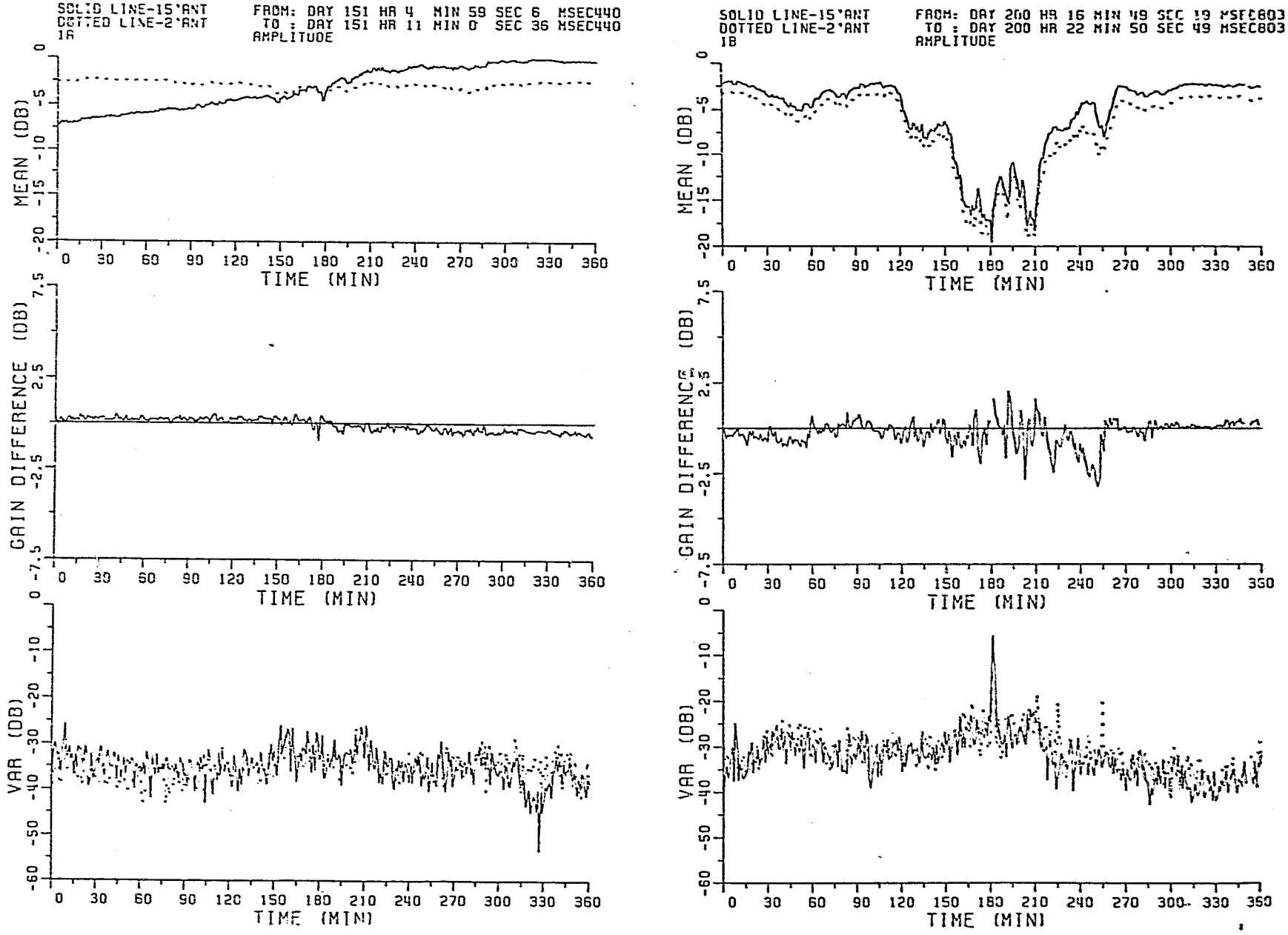

Figure 5. Gain-degradation event records.

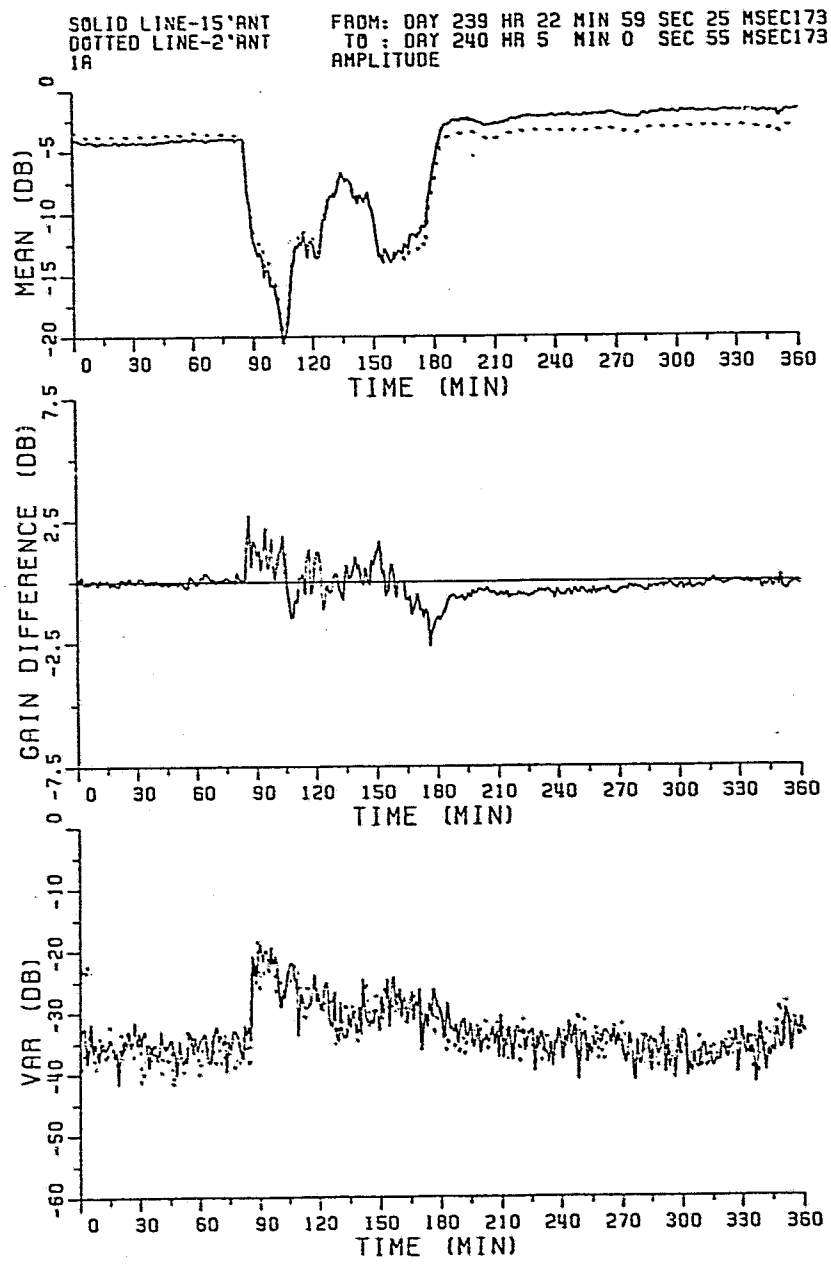

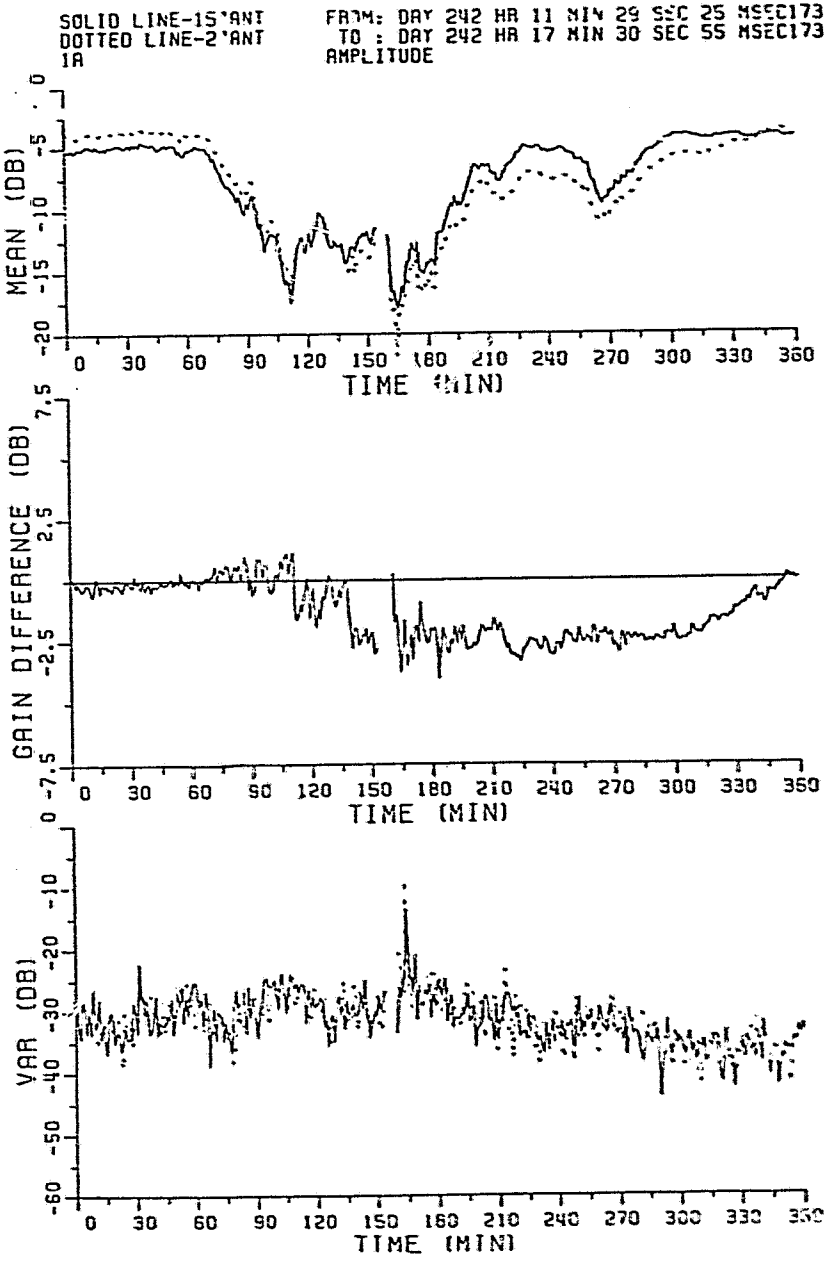

Figure 5. Continued.

The data taken on day 200 includes a period of very deep fading. Gain variations on the order of 1 dB are in evidence during the fading, but most evident is an enhancement of the 5-m antenna signal relative to that of the 0.6m antenna on the order of 1-2.5 dB during a 40-minute period of recovery from the fade. Somewhat similar behavior is exhibited for day 239-240. It should be remembered that an enhancement is a possibility with this system because the antenna was fixed, not tracking the beacon; refraction of the arriving ray in a direction more nearly coincident with the antenna axis would appear as an apparent gain enhancement. Finally, an event of over 3-hour duration appears for day 242.

The long duration of some of these events appears to rule out an explanation in terms of phase scintillations over the aperture. A possible explanation is bulk refractive-index variations associated with the meteorological phenomena which caused the rain or, conversely, caused by the rain. The magnitude of the observed effect (on the order of 2 dB) corresponds to angle-of-arrival variations on the order of 0.1°, which had been observed in an earlier experiment[1]. On the other hand, a gain-degradation experiment conducted at Bell Laboratories at the same frequency during mid-summer 1978 showed no such gain variations [2]. It behooves us therefore, to be very careful to make sure that the effect is not an artifact of the experiment. A first suggestion by the group at Bell Laboratories was that wetting of the antenna windows might be responsible for the long-term apparent gain changes. However, the windows were treated and maintained with Silibond in the manner recommended and used by the Bell Laboratories group and

they were spray-tested during the first installation, in 1980. We intend to repeat the spray tests when the weather moderates; also we are examining the gain degradation record correlation with rain-gauge data to see whether the effect could possibly be attributed to wetting. There are, of course, also other reasons why the Bell Laboratories data might differ from ours, e.g., the brief data period of the Bell Laboratories experiment and the proximity of the seashore which might influence refractive-index structure changes on the scale of several miles, which seem to be implied by our experiment.

It should be noted in Figure 5 that normalized variance levels generally are high during periods of observed gain changes, but that this is equally true for both antenna channels. This suggests that the gain changes are normally accompanied by amplitude scintillations, but not by phase scintillations on a scale smaller than about 5 meters. However, it should be noted that during deep fades, the normalized variances computed by Equation (4) can become large due to the numerator approaching a threshold due to receiver noise. Thus, a more careful analysis, taking receiver noise into account, is required before the correlation of gain changes with amplitude scintillations can be established definitely. Figure 6 shows the relative receiver noise, with respect to the calibration reference level (0 dB) as a function of the relative signal levels. The "noisiness" of the curve is due to the fact that only ten samples were taken at each calibration level. The receiver noise level apparently is 35-40 dB below the reference level.

Figure 7 shows the cumulative distribution of the normalized signal variances. If small-scale phase variations were significant in the experiment, the curves for the two antennas should be distinctly

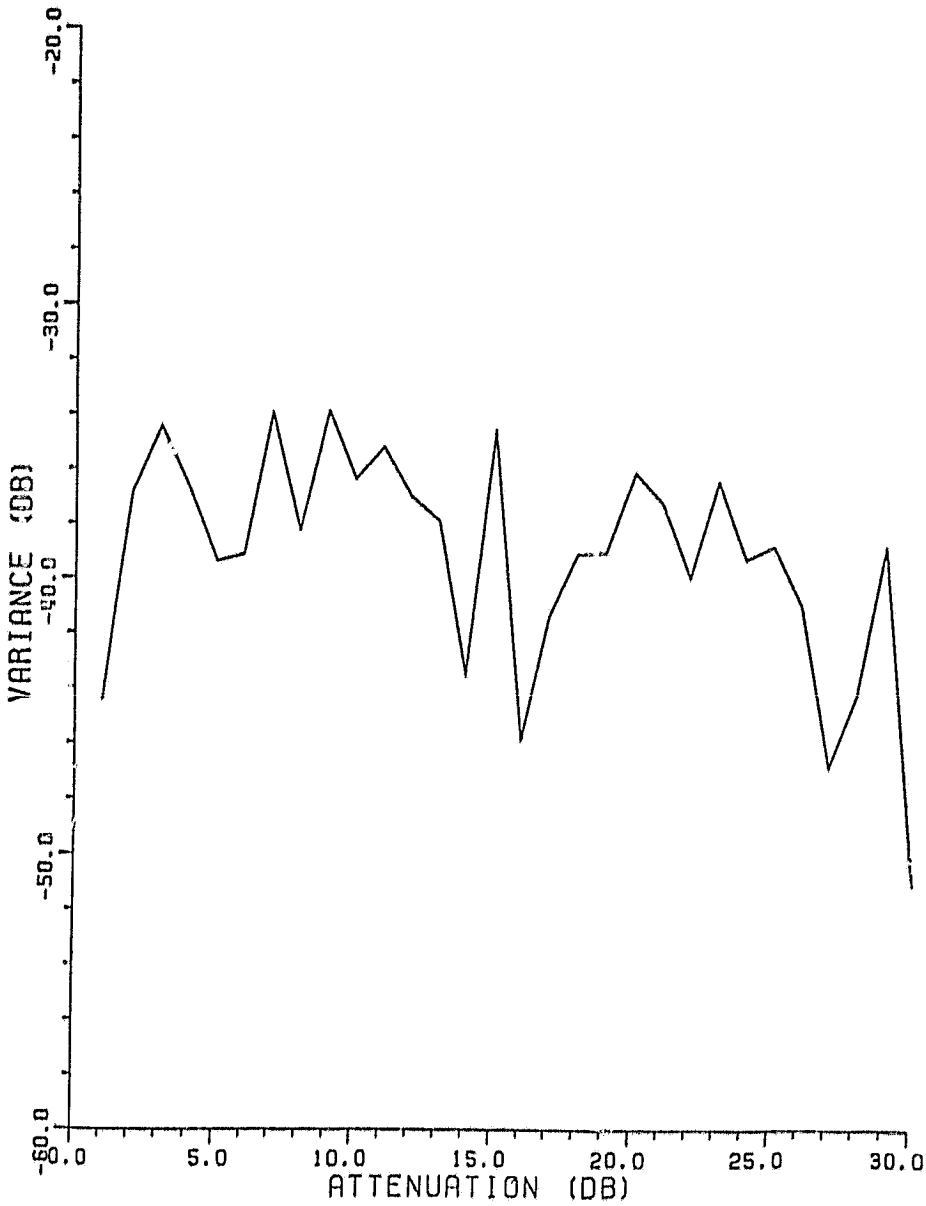

Figure 6. Receiver noise, as observed during the system calibration.

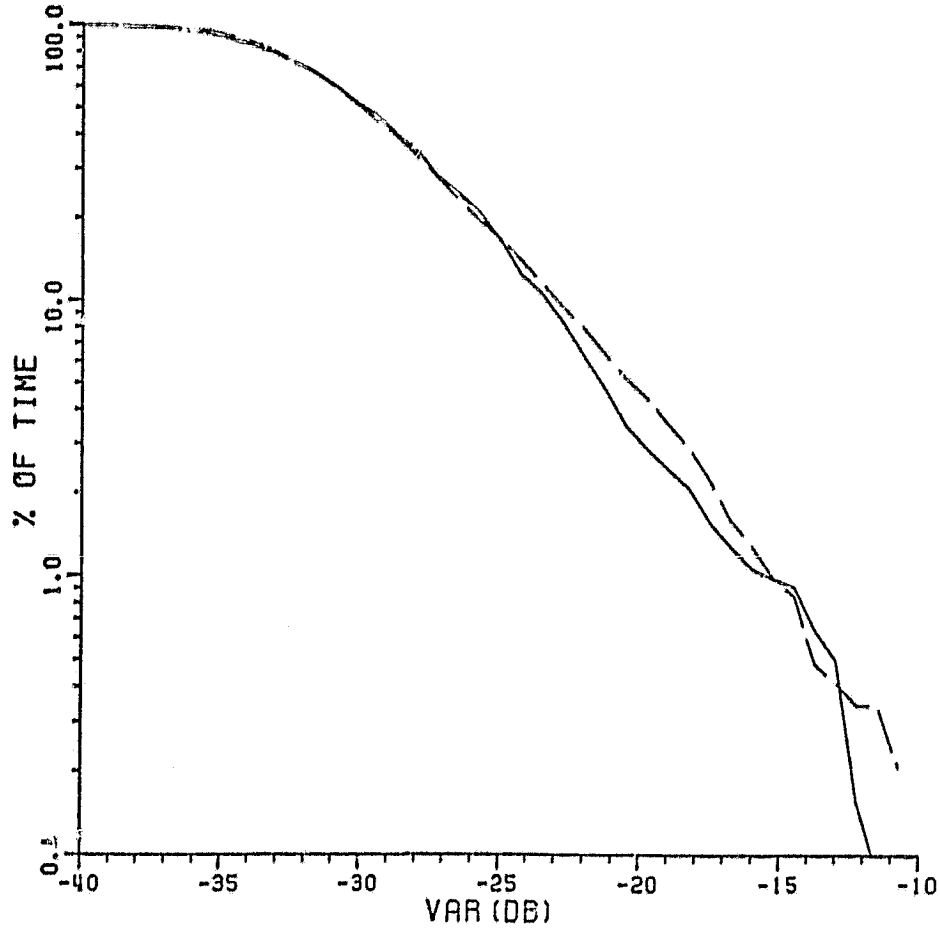

Figure 7. Cumulative statistics of the normalized signal variance.

different. The fact that they are not shows that the observed signal effects must be due to amplitude scintillations and to large-scale (relative to the large antenna aperture), slow phase changes.

A preliminary cumulative gain-change distribution for rain events up to day 161 appears in Figure 8. In this figure, "% of time" refers to the total time for which rain events were deemed to have occurred as 100%, and the gain changes are raw-data derived, i.e., without taking into account how far the satellite position deviated from the array axis at the time of the observation. As before, negative values indicate enhancement of the signal from the large antenna relative to that from the smaller.

Data analysis of this experiment will continue during the remaining two months of the contract.

III. SITE-DIVERSITY RADIOMETRY

A. Purpose of the Experiment

The second task under the contract was to instrument two radiometers at 28.56 GHz, to operate at least one instrument for some time in conjunction with the gain-degradation experiment which monitored the transmission from the Comstar D/4 28.56 GHz beacon, and then to obtain diversity-reception data by means of the two radiometers over as long a period of time as possible. The timing of this task was paced by the expected availability of the D/4 beacon, which ceased operation on 1 September 1981, only 5 1/2 months after the start of the contract. This allowed minimal time for refining a design and procuring the necessary hardware; the design had to be a pre-tested one for which the majority of critical components were already available.

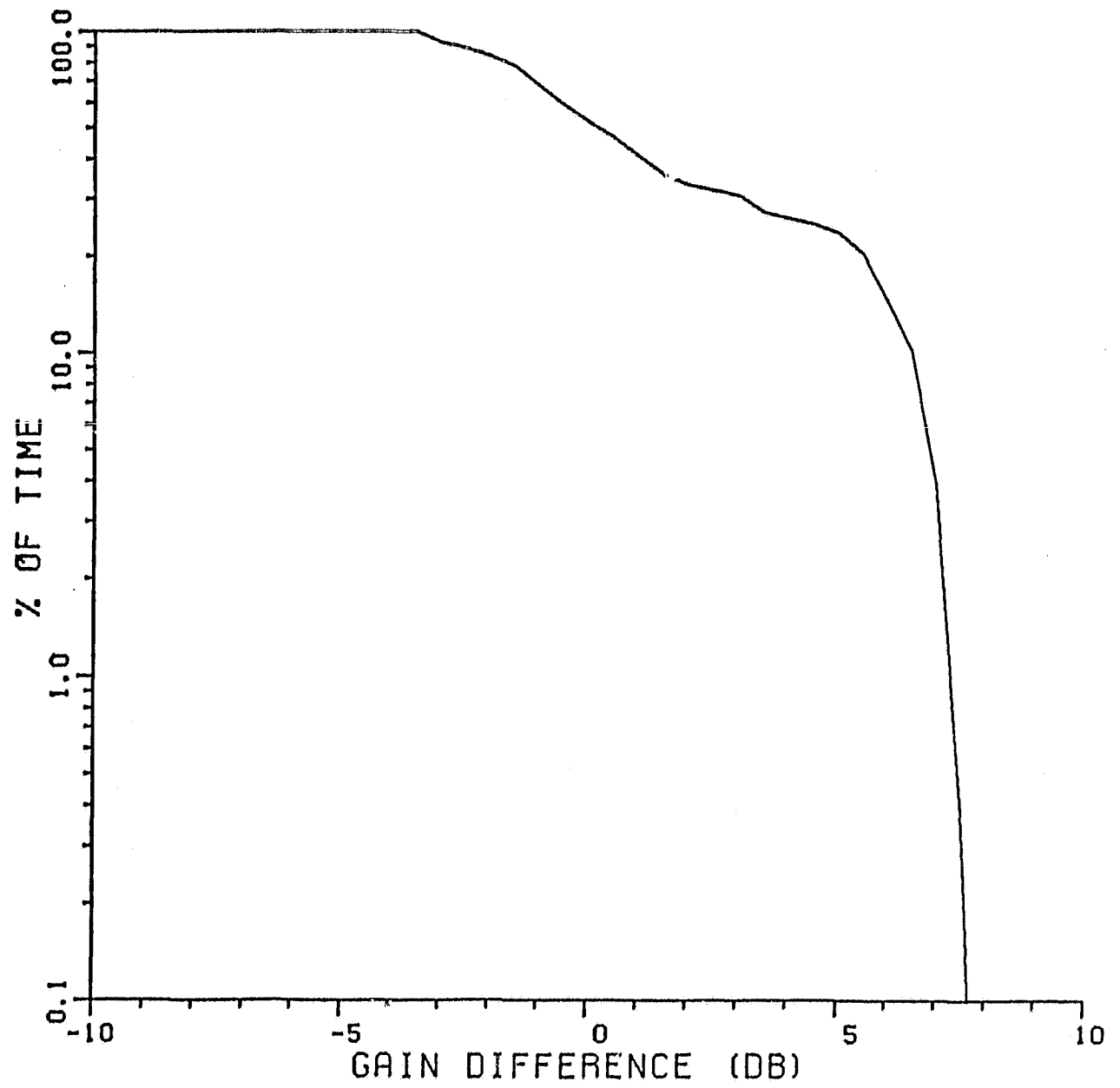

Figure 8. Cumulative gain-change statistics.

B. The Radiometer Systems

A block diagram of the two radiometers, which are essentially identical, is shown in Figure 9. It is an adaptation to this frequency range of a NASA-furnished instrument design [3] and utilizes many of the original components.

The RF front end consists of a Dicke switch in the form of a switchable circulator for modulating the RF signal which is to be synchronously detected in the back end, a three-position waveguide switch to aid system calibration, two waveguide termination ovens and their control circuits for calibration reference temperatures, and a solid state noise source with a waveguide attenuator and directional coupler to provide up-scale reading of system output. A double balanced mixer, with a Gunn diode oscillator input, translates the modulated RF to a 30 MHz IF. The IF is amplified by a broadband amplifier, and an IF filter centered at 30 MHz establishes an 8 MHz bandwidth. The IF signal is envelope detected by a combination amplifier-detector, and the output, now at the Dicke modulation frequency, is amplified, filtered to get only the component at the modulation frequency, synchronously detected, and integrated to get a DC voltage output corresponding to a given effective input temperature to the system. Controls are provided for gain adjustment of the output and phase adjustment in the synchronous detection. Figure 10 is a photograph of one of the radiometer receivers.

This design, like all designs, is a compromise between desirable features and disadvantages. A real advantage is the ease of

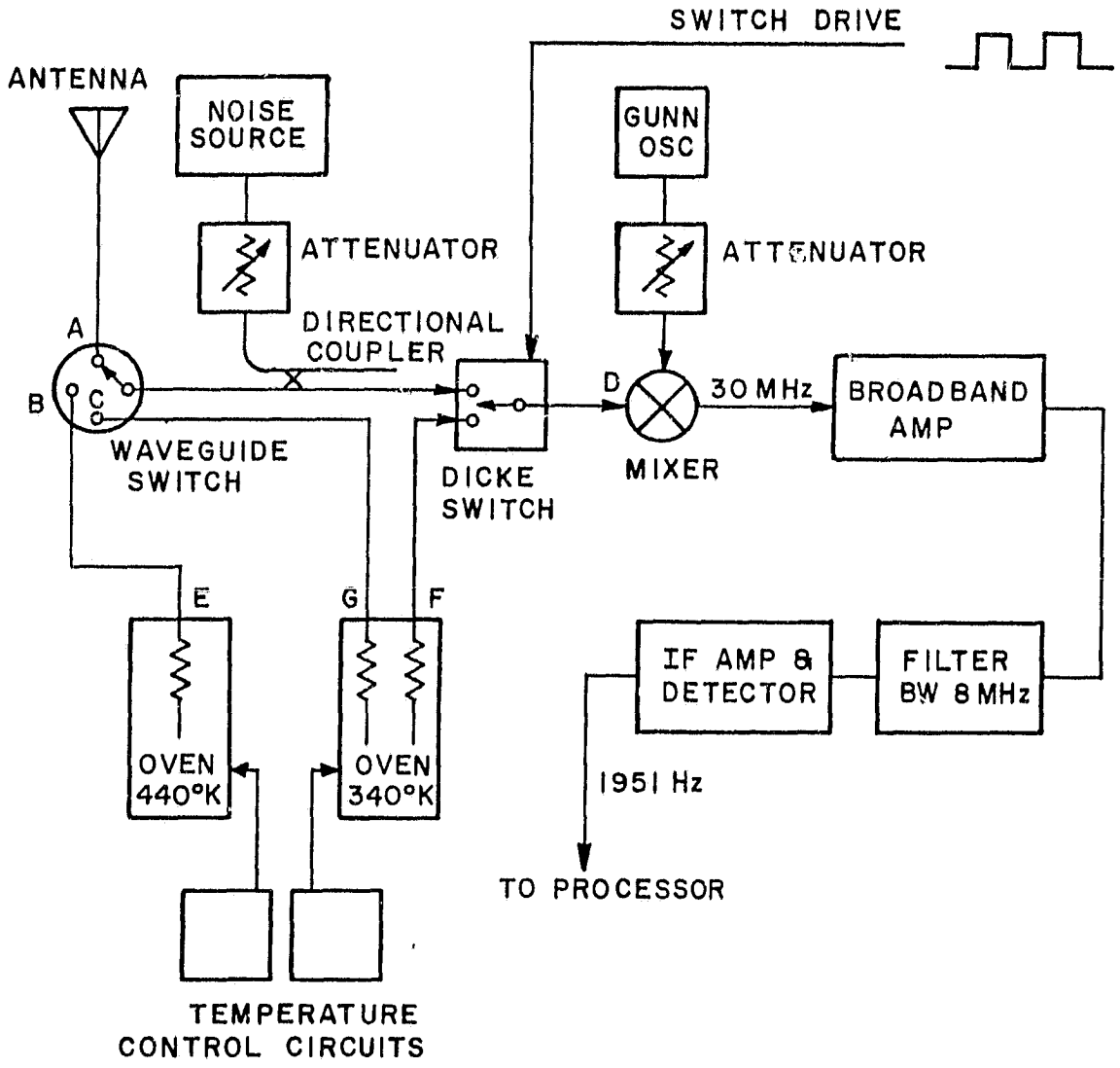

Radio-frequency

Figure 9. 28.56 GHz radiometer block diagram, a) Radio-frequency circuits, b) processor.

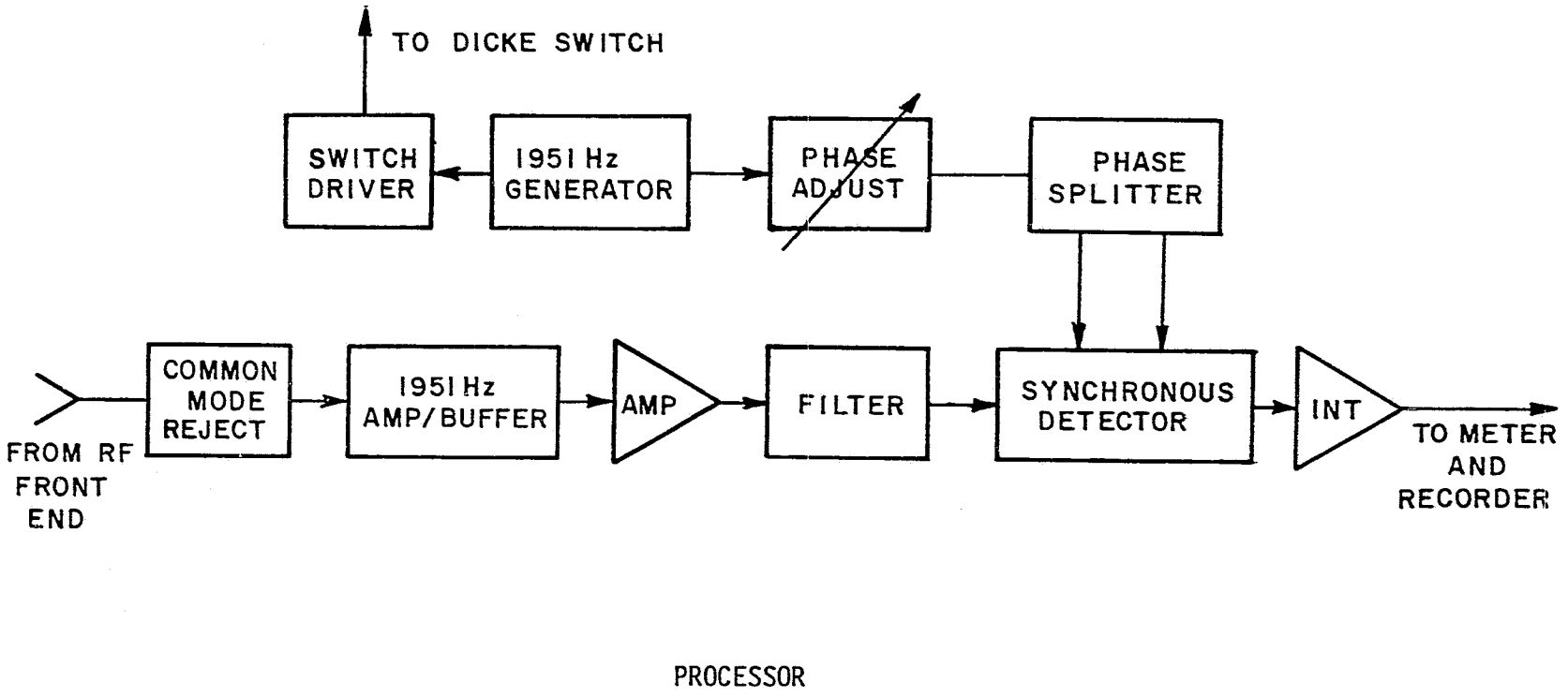

Figure 9. Continued.

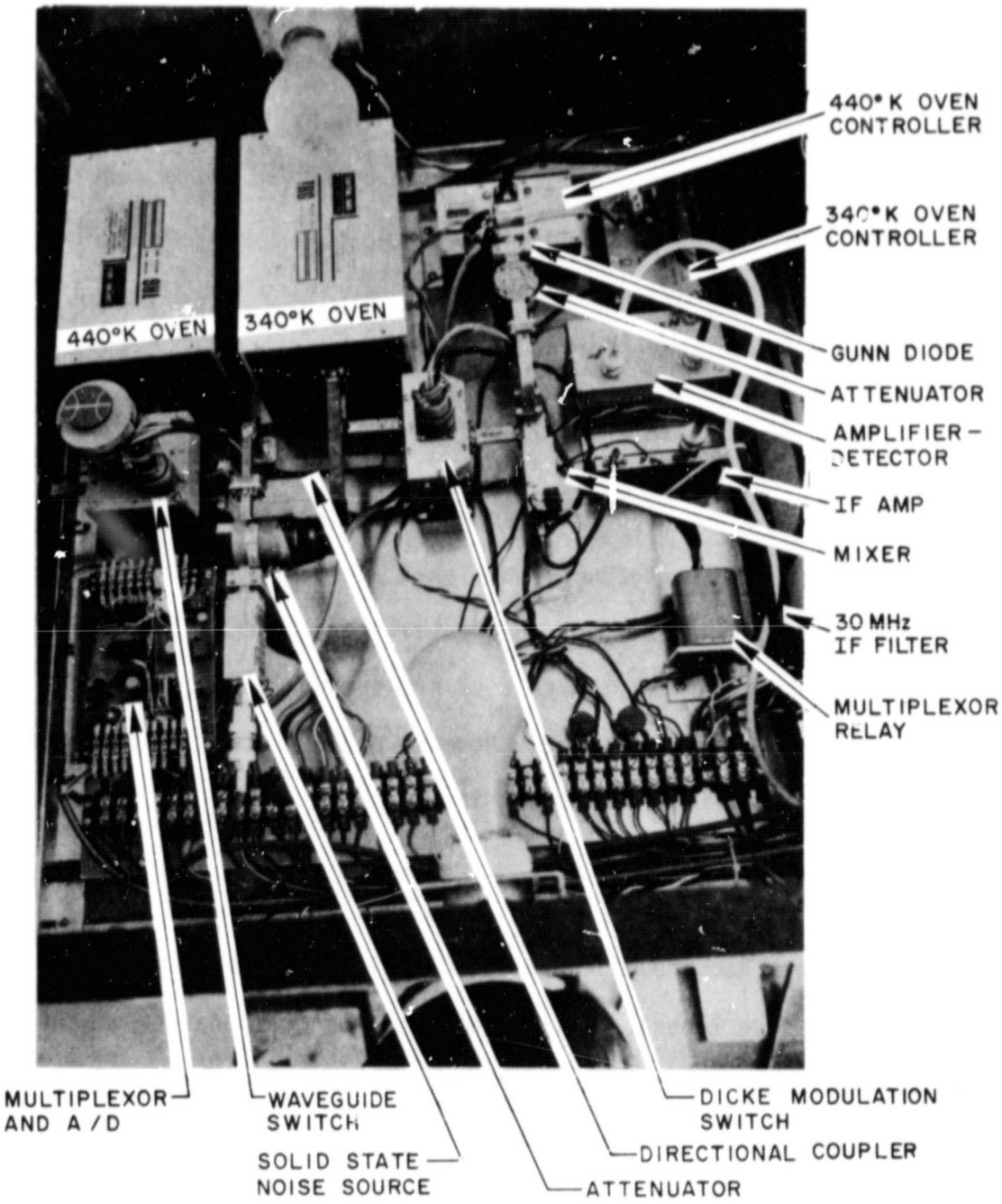

Figure 10. Radiometer receiver.

checking calibration by transferring the receiver input from the antenna by means of the waveguide switch to either of two temperature-regulated loads. The corresponding disadvantage is the loss in the switch and in the longer waveguide runs and the increased number of bends required by use of the switch. These losses require a careful measurement of the temperature of the lossy components during operation as well as a careful system calibration for good accuracy, as discussed below.

C. Radiometer Calibration

To understand the need for accuracy, the relationship between radiometric antenna temperature and signal loss over a satellite-earth path needs to be discussed. At 28 GHz that relationship involves both absorption and scattering; the role of scattering is discussed in considerable detail in Section E. Here we neglect scattering in order to develop an approximate relationship

$$T_{ant} = T_{back} + T_m (1-t) \qquad (7)$$

where T_{back} is a background temperature (primarily energy picked up from the ground by side lobes), T_m is a weighted mean temperature of the transmission path, and t is the fractional transmission over the path. This relation can be solved for t:

$$t = (T_m - T_{ant} + T_{back})/T_m \quad . \qquad (8)$$

A plot of the transmission loss in decibels, $L = -10 \log_{10} t$, is plotted in Figure 11, with assumed values of 30 K for T_{back} and 270 K for T_m. It is apparent that very little accuracy in the antenna temperature is

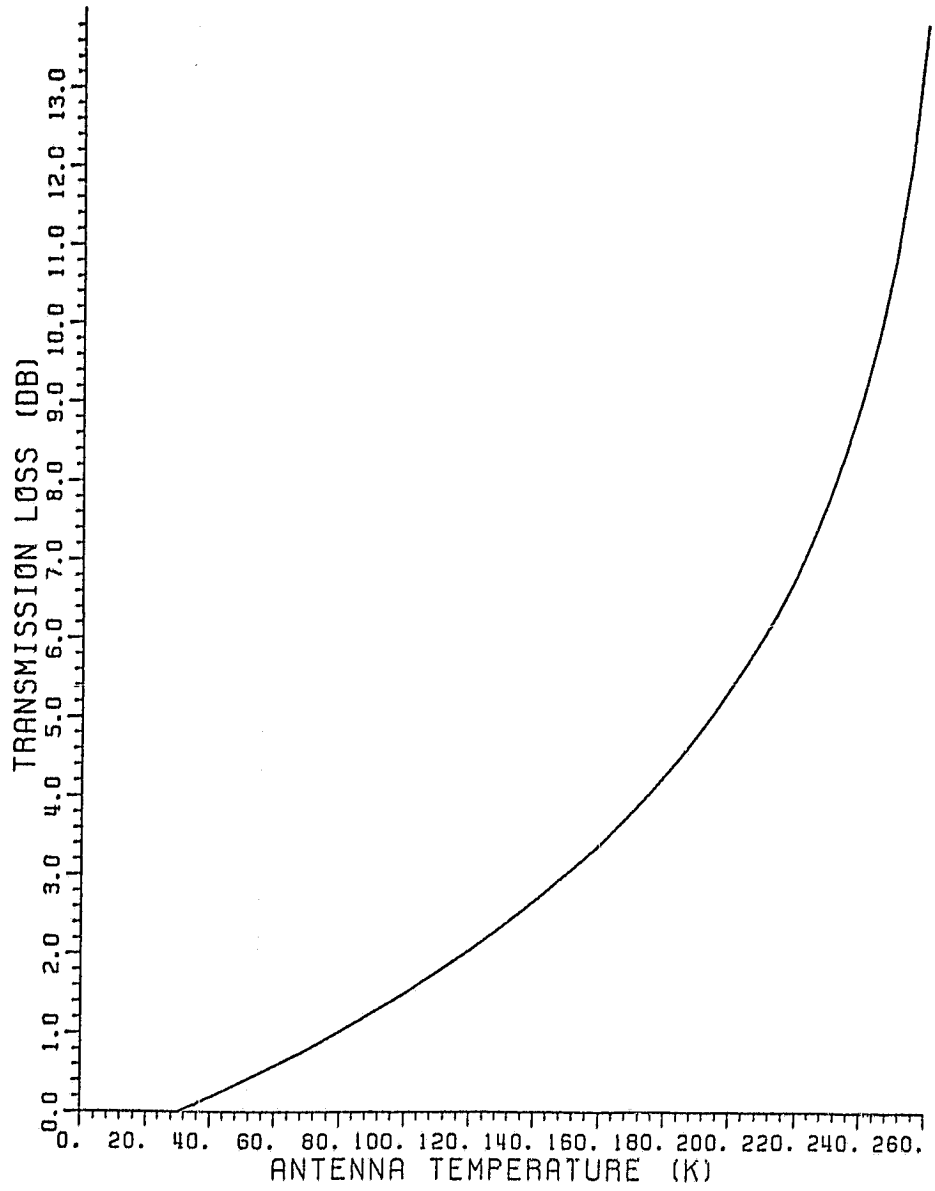

Figure 11. Transmission loss vs. antenna temperature. A background of of 30 K and weighted path mean temperature of 270° is assumed.

required for small transmission losses, but the accuracy requirement increases for higher transmission losses. Ultimately the fade depth which can be inferred reliably from the radiometric measurement is therefore limited by the accuracy with which the antenna temperatures can be measured. The value of T_m normally is derived from the measurements and therefore is itself also dependent on the measurement accuracy.

The effective temperature at the Dicke switch input is related to the antenna temperature by an equation similar in form to Equation (7)

$$T_{eff} = \alpha T_{ant} + (1-\alpha)\, T_{amb} \qquad (9)$$

where α is the transmission factor for the waveguide path and T_{amb} is the ambient temperature of the waveguide components. Similar relations apply when the waveguide switch is switched to the heated loads for calibration, in which case the physical temperature of the load replaces T_{ant}.

The ideal calibration procedure would measure the noise temperature of a precisely calibrated variable standard noise source. Unfortunately no such sources are available; practical solid-state noise sources in this frequency range normally are expected to maintain calibration only to within approximately 3 dB. We therefore used a calibration procedure which utilized the two temperature-controlled hot loads and an ambient or, on occasion, ice-water cooled load as standards.

First, all terminations were checked for VSWR and all losses were measured. Next the 440 K oven was connected to the input by means of the waveguide switch with the noise source turned off. From the known load temperatures, waveguide losses, and ambient temperature, the

effective temperature difference at the Dicke switch output port was calculated and the amplifier gain was set to produce an output voltage corresponding to 0.02 Volts/Kelvin. The waveguide source and precision attenuator were then substituted for the 440 K oven and calibrated by adjusting the precision attenuator until the radiometer output matched that previously obtained with the 440 K oven; the temperature of the noise source could then be calculated from the attenuator setting, taking into account its ambient temperature contribution. The noise-source attenuator combination therefore could be used as an accurately calibrated noise source to check system linearity. Finally, the noise source was reconnected to the directional coupler, the 440 K oven was connected to the input, and the noise source attenuator was adjusted so as to make an effective temperature of 100 K correspond to zero output. The cold load was then used as an additional check on the system calibration.

When the first radiometer was finished in July, the calibration procedure yielded results which were not mutually consistent within the inherent accuracy expected of the instrument. The problem has since been traced to a failure of one of the waveguide hot loads, which cracked and separated from the thermocouple, thus giving incorrect temperature readings and also raising the VSWR slightly. At the time, we were faced with a choice, on one hand, of taking the time to locate and fix the fault and do a thorough calibration and ending up with less data during the D/4 beacon life or, on the other, to operate with a somewhat questionable calibration but longer data period for collecting data while the beacon was still in operation. We chose the second

option. As a consequence we did obtain data for 5 significant rain events with both the radiometer and the beacon-reception systems, but this data has to be analyzed with considerable care in light of what we learned about the oven afterward. This data analysis phase is just beginning.

Work on the second, remote-site, radiometer started in mid-August. An effort was made to minimize path losses. A slotted line was used to check that all VSWR's were satisfactory for waveguide and termination load ovens. The 440 K calibration oven appeared to be badly mismatched, so we were forced to replace it with a K-band oven. A waveguide transition piece was necessitated by the substitution to connnect the oven's waveguide flange to the system's smaller flange. All the waveguide path losses were measured using a power meter and a microwave source on two separate occasions with good agreement. Again, satisfactory linearity checks were made, once of the complete system with the solid state noise source and precision attenuator as an input noise temperature, and once of the amplifier section with a 30 MHz source externally AM modulated by the Dicke modulation drive as the IF input to the amplifier following the mixer. The calibration of the remote-site radiometer went smoothly, without any serious difficulties or contradictions, but we saw again the importance of knowing path losses and oven temperatures very closely. The calibration curve for the second radiometer is shown in Figure 12.

A data acquisition system for transmission of data via telephone lines from the remote-site radiometer was developed; it also controls the remote radiometer functions. A multiplexing scheme is used prior to

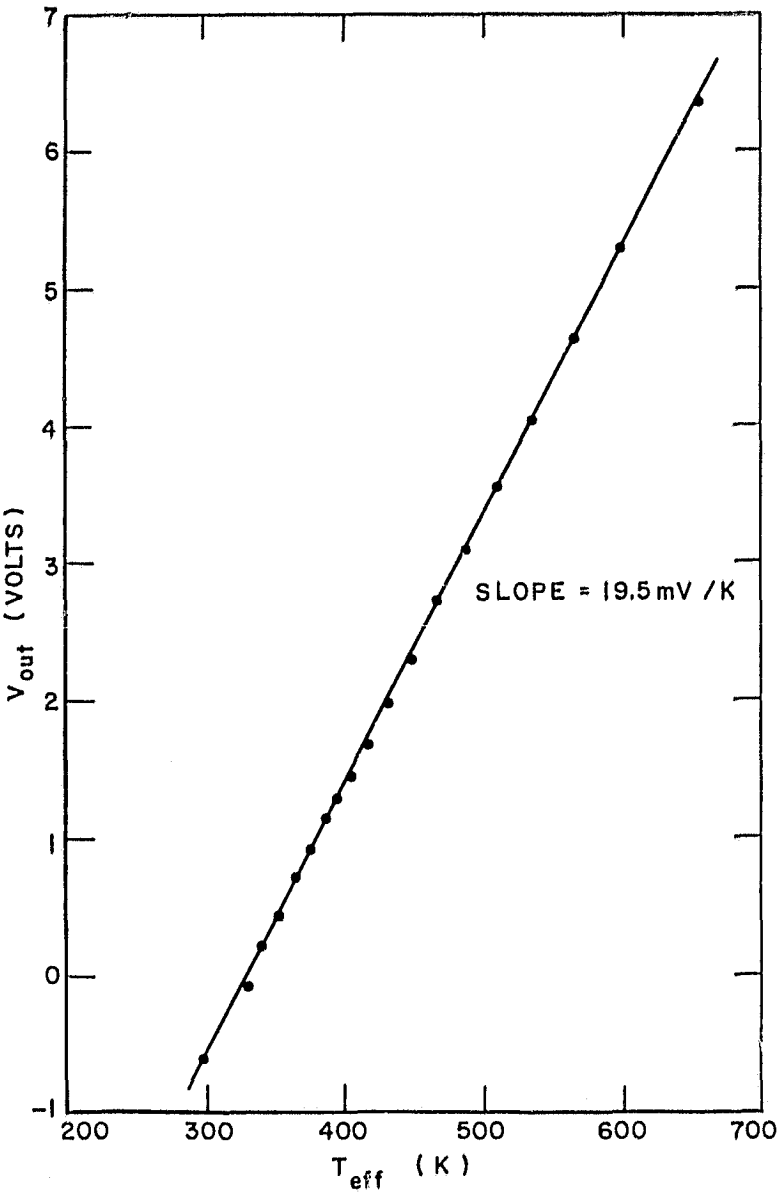

Figure 12. Radiometer calibration curve.

digitizing the data. The radiometer voltage and the oven thermocouple wire voltages and ambient temperature indicator voltage are transmitted to the main site and recorded on magnetic tape. The latter voltages indicate absolute ambient temperatures inside and outside the box enclosing the front-end equipment. The inside temperature is kept within limits in cold weather by means of light bulbs installed as heaters in the front-end box.

D. Current Operational Status

The remote radiometer, installed in a truck, is scheduled to be installed at its prepared site just west of the University Airport, at a distance of 9.03 km and bearing of 337° 45' from the main site. Meanwhile, since 440 K loads in WR-28 waveguide are not commercially available, a new load has been built and tested for the main site radiometer and this radiometer has been recalibrated. Diversity operation should commence in the very near future.

E. The Role of Scattering in the Interpretation of Radiometric Brightness in Terms of Transmission Loss

In a linear but not necessarily homogenous medium the power removed per unit distance from a propagating wave is proportional to the local power density,

$$\frac{dP(\ell)}{d\ell} = [K_a(\ell) + K_s(\ell)]\, P(\ell) = K_e(\ell)\, P(\ell) \,, \qquad (10)$$

where the first term in the middle of the equation represents the power removed by absorption and the second term the power removed by

scattering. The function $K_a(\ell)$ is known as the absorption coefficient, the function $K_s(\ell)$ as the scattering coefficient, and their sum K_e as the extinction coefficient. The power decrease over a distance L is found by integration to be governed by

$$P(0) = P(L)\, e^{-\tau(L)} \tag{11}$$

where the optical depth is given by

$$\tau(\ell) = \int_0^{\ell} K_e(\ell')\, d\ell' \quad , \tag{12}$$

with the wave traveling from ℓ=L towards ℓ=0. If a brightness temperature T_b is defined by

$$P = k_B T_b B \tag{13}$$

where k_B is Boltzmann's constant and B the system bandwidth, Equation (12) becomes

$$T(0) = T(L)\, e^{-\tau(L)} \tag{14}$$

for a wave propagating through the medium. However, thermo-dynamic considerations dictate that an absorbing medium at non-zero absolute temperature also emits energy according to the law

$$dT_{em}(\ell) = T\,(\ell)\, K_a(\ell)\, d\ell \tag{15}$$

where T_{em} represents the emission brightness temperature and T the physical temperature of the medium. This emitted power also is attenuated on its way to the receiver, so that a receiver on the ground

sees a brightness temperature

$$T_b(0) = T_{sky}\, e^{-\tau(L)} + \int_0^L T(\ell)\, K_a(\ell)\, e^{-\tau(\ell)} d\ell \qquad (16)$$

where L now represents the effective path length through the atmosphere. The intrinsic sky brightness at 30 GHz is approximately 14 K; it and energy picked up by sidelobes from the warm ground account for the background temperature in Equation (7). We shall ignore this relatively constant contribution for the moment and deal with the effective brightness contribution

$$T_{be} = T_b - T_{back} = \int_0^L T(\ell)\, K_a(\ell)\, e^{-\tau(\ell)} d\ell \quad . \qquad (17)$$

When scattering is insignificant, as it is at frequencies below about 10 GHz, one obtains

$$K_e(\ell) = K_a\ (\ell) \qquad (18)$$

and the term multiplying $T(\ell)$ in Equation (17) becomes an exact differential. Integration by parts then gives

$$T_{be} = T(0) - T(L)e^{-\tau(L)} + \int_0^L \frac{dT(\ell)}{d\ell}\ e^{-\tau(\ell)} d\ell \quad . \qquad (19)$$

If the temperature is uniform, this reduces to

$$T_{be} = T[1-e^{-\tau(L)}] \quad . \qquad (20)$$

When T is not uniform, since the term multiplying T (ℓ) in Equation (17) is uniformly positive, one can still write

$$T_{be} = T_m\,[1-e^{-\tau(L)}] = T_m[1-t] \tag{21}$$

where T_m is a weighted average of T over the path, the weight being $k_a(\ell)e^{-\tau(\ell)}$. The variation of T over the rain-attenuation part of the path is generally small, say from 273 K at the melting layer to 300 K at the ground for a typical Ohio convective storm. It is therefore not surprising that experimental data are often approximated well by Equation (21) which implies Equation (7), and the path loss 1/t can be inferred from the radiometric temperature by use of that equation, subject to the accuracy limitations discussed above.

When scattering is included, the absorption and extinction coefficients are no longer equal. However, we can set

$$K_s(\ell) = k(\ell)\,K_a(\ell) \tag{22}$$

and obtain from the second equality of Equation (10)

$$K_a(\ell) = [1 + k(\ell)]^{-1}\,K_e(\ell) \tag{23}$$

so that Equation (17) can be written as

$$T_{be} = \int_0^L T(\ell)[1+k(\ell)]^{-1}\,K_e(\ell)e^{-\tau(\ell)}\,d\ell\ . \tag{24}$$

Analogously to Equation (21), this results in

$$T_{be} = \overline{T/(1+k)}\,[1-e^{-\tau(L)}] = \bar{T}_m(1-t) \tag{25}$$

or

$$t = \frac{\bar{T}_m - T_{be}}{\bar{T}_m} \tag{26}$$

where $\bar{T}_m = \overline{T/(1+k)}$ is a weighted average (weight $K_e(\ell)e^{-\tau(L)}$) of the factor $T(\ell)/[1+k(\ell)]$ in Equation (24). The question is how well this weighted average can be predicted or inferred from the experimental data. We noted before that $T(\ell)$ is rather well bracketed; the situation with respect to $k(\ell)$ is not so clear. Our approach therefore is to calculate k for various rain rates and to compute, by Equation (24), the effect of its variation along paths with assumed rainrate distributions. This will elucidate the limitations on the deduction of path loss by means of Equation (26). In addition, we can use some of the actual rainrate distributions along the path as measured by the radar. This was one of the main reasons for keeping the radar in operation beyond the time required for the Intelsat program.

The absorption, scattering, and extinction coefficients are given respectively by

$$K_a = \int_0^\infty C_a(r)\, N(r)\, dr \tag{27}$$

$$K_s = \int_0^\infty C_s(r)\, N(r)\, dr \tag{28}$$

$$K_e = \int_0^\infty C_e(r)\, N(r)\, dr \tag{29}$$

where the C's are the cross sections for absorption, scattering, and extinction, respectively, for single drops of radius r and N(r) is the number density of such drops. The cross sections are calculated from

$$C_e = \frac{\lambda^2}{2\pi} \sum_{n=1}^{\infty} (2n+1)\ \mathrm{Re}(a_n+b_n), \tag{30}$$

$$C_s = \frac{\lambda^2}{2\pi} \sum_{n=1}^{\infty} (2n+1)\ (|a_n|^2 + |b_n|^2) \quad , \tag{31}$$

$$C_a = C_e - C_s \ , \tag{32}$$

where the a_n and b_n are the usual coefficients of the Mie series. Programs for calculating C_e have been available at this Laboratory, they have now been modified to yield also C_s and C_a. The program AEROSOL,[4] written at the Air Force Geophysics Laboratory is also being adapted to our VAX 11/780. In addition the programs MIEV0 and MIEV1 written by Wiscombe at NCAR [5] have been requested. This will allow a careful check of the adequacy of the Mie calculation, a precaution that seems wise because the series term generation algorithm (specifically, at what radius to break between upward and downward recursion) depends on frequency both directly and via the complex refractive index.

So far the program has been used with the Marshall-Palmer exponential drop-size distribution. A recent report of the CCIR [6] calculates K_e and K_a as a function of frequency for a rain-rate of 12 mm/hr using a drop-size distribution which is given only in numerical form. A comparison of the curves from the CCIR report and ours (corresponding to the exponential distribution) appears in Figure 13. The agreement is not as good as would be desirable. We are therefore in the

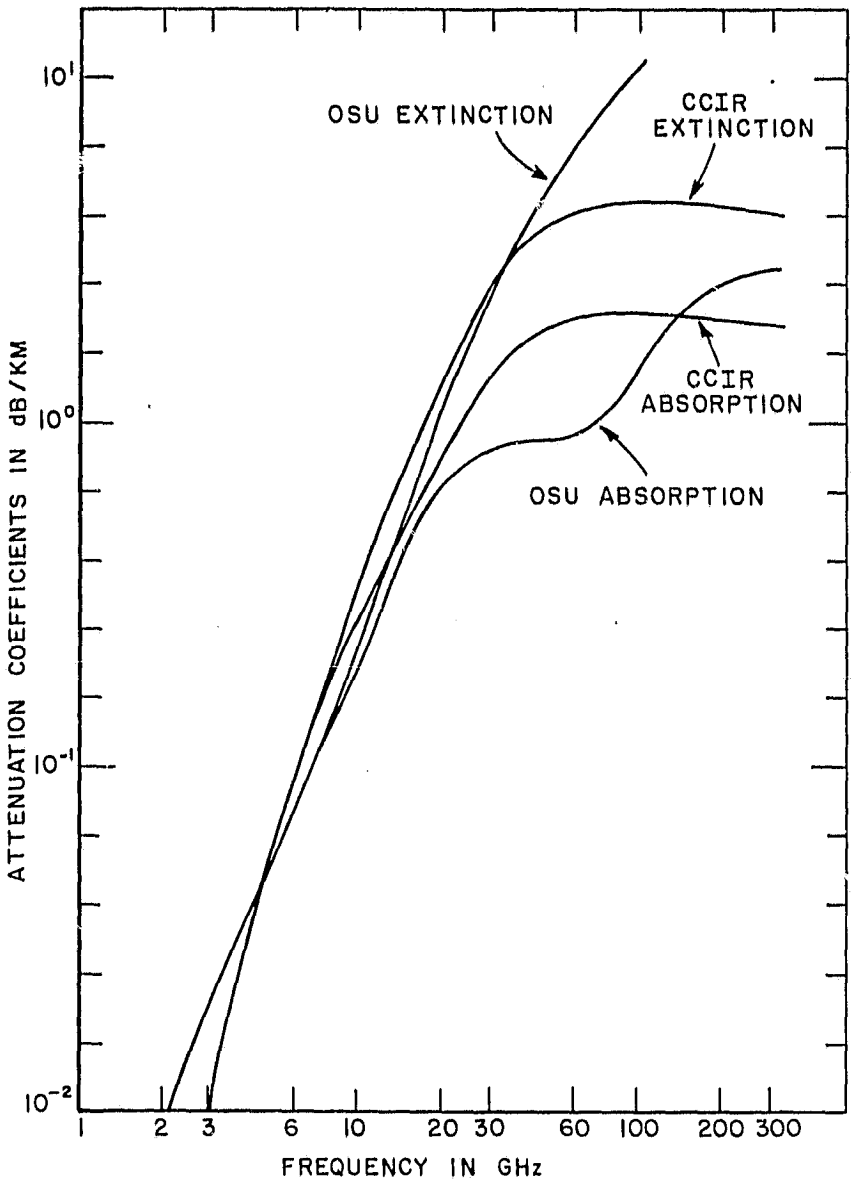

Figure 13. Extinction and absorption coefficients for a rain rate of 12 mm/hr. The data labeled CCIR is taken from reference [6]; OSU denotes our computations.

process of programming the CCIR-specified distribution to see whether the drop-size distribution is so critical to the calculation, or whether there are other bugs in the program. It is expected that this question will be resolved shortly. The program for performing the integration of Equation (24) is in progress, and it is expected that at least rough calculations of the relationship between radiometric temperature and extinction in the presence of scattering will be available by the end of the contract period.

IV. THE UPGRADED SITE-DIVERSITY GAIN MODEL

The revision of the diversity-gain model has been completed, and a separate technical report on this subject has been delivered [7]. It has also been submitted as a paper for Radio Science. The diversity gain is represented in the form

$$G_D = G_d G_f G_\beta G_\Delta \quad . \tag{33}$$

The most significant contribution is given by the factor

$$G_d = a(1-e^{-bd}) \quad , \tag{34}$$

$$a = 0.64A - 1.6(1-e^{-0.11A}) \quad , \tag{35}$$

$$b = 0.585\ (1-e^{-0.098A}) \quad , \tag{36}$$

where d is the baseline distance in km and A the single-site fade depth in dB. The frequency correction factor is

$$G_f = 1.64\ e^{-0.025f} \tag{37}$$

where f is expressed in GHz. The elevation-angle correction factor is

$$G_\beta = 0.00492\beta + 0.834 \tag{38}$$

where β is expressed in degrees. The baseline-orientation factor G_Δ is given by

$$G_\Delta = 0.00177\Delta + 0.887 \tag{39}$$

where Δ is the acute angle between the baseline and the projection of the propagation path onto the surface of the earth, in degrees. The reader is referred to the technical report [7] for details.

V. DATA ACQUISITION SYSTEM

A. Background

The current data acquisition system was designed and constructed around 1975. This system was not well documented at that time, and many modifications have been made, some of which are not documented at all. The system is quite reliable, but when a problem does occur it is very hard to trouble-shoot, due to a lack of good documentation. The system employs two minicomputers: an LSI-2 which is poorly supported in terms of repairability and trouble-shooting, and an HP 2116B which is no longer fully supported by the manufacturer but for which we have good diagnostic software, spares, and a second identical unit for back-up. At present the HP 2116B is used in a mode which emulates a second LSI-2.

In an attempt to correct this problem, a new data acquisition system was designed and built around an AIM-65 microcomputer. It was anticipated that this system would provide better documentation, be easier to modify, interact better with the operator, be more reliable and would be easier to trouble-shoot. Unfortunately, the anticipated advantages were not realized due to several problems with the AIM system. The main problem is the lack of commercially available interfaces to run the peripherals. The required interfaces were built in-house and they are not as reliable as is required. More reliable boards could be built with some effort. Another problem with the AIM is the lack of good documentation and of diagnostic software for this processor.

The AIM is not easily interfaced to a magnetic tape drive. This means a complex board must be built to interface the tape drive. Since the tape drive is a very important link in the data path of the system, this board also must be very reliable.

The main problem is that the AIM 65 does not appear to be itself a highly reliable machine. A presumably more reliable industrial version, designated RM-65, has been introduced; its performance is not known to us at present. No self-diagnostic programs come with these microprocessors.

For these reasons it has been decided to redesign the system around the HP 2116B because of its high reliability, good diagnostic software, and manufacturer-built interface boards. In a sense, this is a stop-gap measure because the aging HP 2100 series is no longer fully supported by the manufacturer. However, with our back-up spare unit and additional

spare parts, it should be possible to operate the system for several years with very little trouble.

B. Proposed Configuration

The changes in the hardware will mostly be in the way that peripherals are interfaced to the 2116B. The current system has the magnetic tape interfaced through the LSI-2 mini-computer. The LSI-2 will be removed and the interfacing will be done directly. At present, the modem and A/D circuitry is interfaced through a device that emulates a LSI bus. This emulater will be removed and the device driven directly by the HP-2116B. The proposed hardward configuration is shown in Figure 14.

The software will be rewritten completely; it will be more modular and will localize the I/O more so that the system will be easier to modify. The tape record format will be modified to save tape and make the records easier to read. The interrupts will be used only to service the specific device that caused the interrupt; this will reduce the chance of a conflict between interrupt routines. The software is tentatively being designed as a multi-processing program, but a serial dispatcher will be used to eliminate most of the problems that multi-processing can encounter.

One of the questions one faces when designing a software system is whether the system should be written using several concurrently executed programs or one sequential program. When several concurrent programs are used, the programs all appear to be running simultaneously. This is

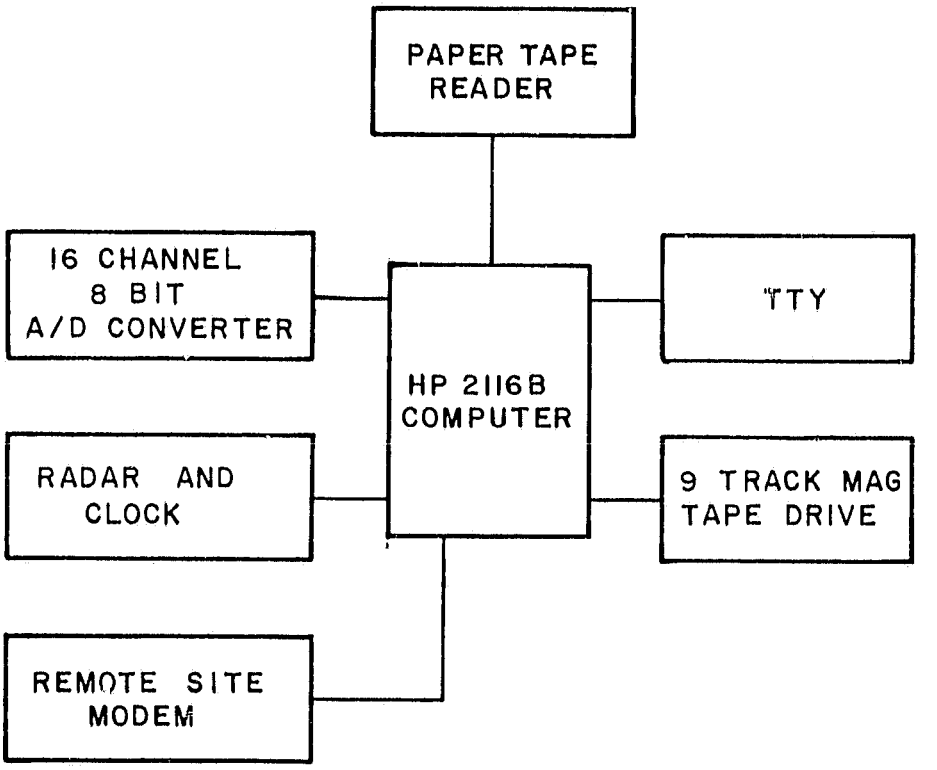

Figure 14. Proposed hardward block diagram.

a great advantage in a real-time system because two or more independent jobs can be done at once. Also it allows the programmer to divide a complex job into several simple and independent jobs, each small enough so that they are quite easily programmed. Concurrent programming also has some disadvantages. One problem is passing data between two jobs, since one job may not want to receive the data when the other wants to send it. Another problem is debugging the program, due to the fact that all these jobs are not executed sequentially. The last problem is the fact that not many high level languages support concurrent programming; this means that much of the program might have to be written in assembly language. Despite the disadvantages, our current efforts tentatively lean toward concurrent programs.

The software is shown in block diagram form in Figure 15. The data is sampled by the data device drives on request from the data sampler. The data sampler combines the data into a sample unit that is sent to the record writer. The record writer combines sample units until a complete record is formed, at which time it requests the magnetic tape driver to write it onto the tape. Any commands from the user will enter the user interface via the TTY driver. The user interface will then tell the control what needs to be done.

Currently the task performed by each block is being specified; this should be complete by the second week in April. At that time the software will be coded. This should be completed by the end of June. The system should be ready for initial debugging by midsummer.

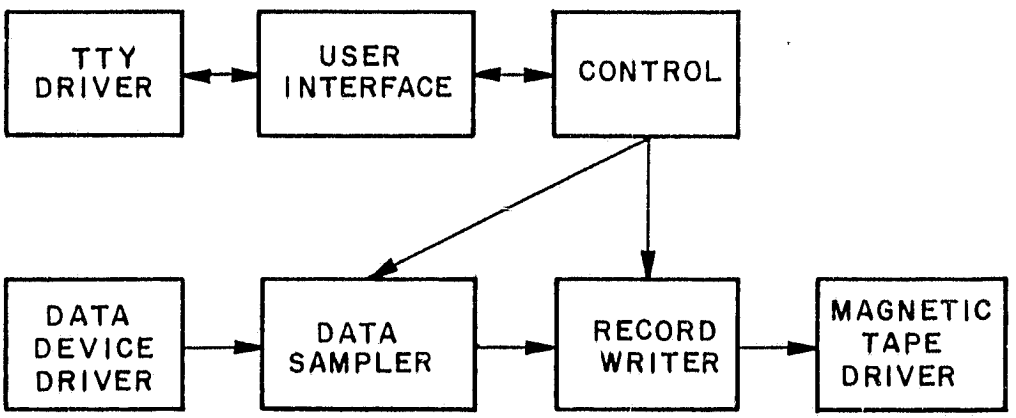

Figure 15. Proposed software block diagram.

VI. TECHNICAL REPORTS ISSUED AND IN PREPARATION

The current contract is a follow-on of Contract NASW-3393. Not all work under that contract had been documented fully at the beginning of the current contract period. The following technical reports pertaining to the earlier tasks were issued.

D.M.J. Devasirvatham and D.B. Hodge, Amplitude and Angle of Arrival Measurements on a 28.56 GHz Earth-Space Path, Report 712759-4, March, 1981.

T.C. Lee and D.B. Hodge, The Comstar D/3 Antenna Gain Degradation Experiment, Report 712759-5, June, 1981.

D.M.J. Devasirvatham and D.B. Hodge, The Effects of Turbulence on Microwave and Millimeter Wave Satellite Communications Systems, Report 712759-6, June, 1981.

B.W. Kwan and D.B. Hodge, Amplitude and Angle of Arrival Measurements on a 28.56 GHz Earth-Space Path During 1979-80, Report 712759-7, June, 1981.

The following technical report pertaining to the tasks under the current contract has been issued:

D.B. Hodge, An Improved Empirical Model for Diversity Gain on Earth-Space Propagation Paths, Report 713656-1, September, 1981.

The following detailed technical report should be ready about July 1, 1982:

K.T. Lin, C.A. Levis, R.C. Taylor, A 28-GHz Antenna Gain Degradation Experiment.

The diversity radiometry experiment and the associated analysis of the role of scattering are topics pursued as theses by Mssrs. Pigon and Leonard, who are associated with this program as University Fellows. Their theses should be issued as technical reports about August 1982:

B. Pigon, Radiometrically Inferred Site-Diversity Attenuation: Calibration and Initial Results.

R. Leonard, The Role of Scattering in Inferring Path Loss from Radiometric Brightness Above 10 GHz.

VII. CONCLUSIONS

A new empirical model for site-diversity gain has been developed. It incorporates the dependence on single-site attenuation, site separation, frequency, base-line orientation with respect to the propagation path, and elevation angle. The last three dependencies were found to be relatively weak.

The antenna-gain degradation experiment using the Comstar D/4 satellite 28.56 GHz beacon shows evidence of substantial gain changes as a result of rain events. The time scale is such that bulk refractive effects, rather than phase scintillations over portions of the 15-foot

aperture, are involved. The data analysis is not yet complete, and the conclusions should be viewed as tentative.

A diversity-radiometry experiment has been implemented and calibrated. The calibration involved careful measurement of system losses and continuous monitoring of the temperature of the lossy components. Calculations to show the effects of scattering on the interpretation of radiometric brightness in terms of path loss over a satellite-to-earth path are underway utilizing the Mie series formulation and appropriate drop-size distributions.

The attempts to insure future reliability of our data acquisition system by utilizing an AIM-65 microprocessor as central to the system were not successful. New software and interfaces for the HP2116B-based acquisition system are being developed for this purpose.

VIII. RECOMMENDATIONS

The site-diversity radiometry experiment should be continued until at least a full year of data has been accumulated. The analysis of scattering effects should be concluded.

The analysis of the 1981 gain-degradation should continue. While the experiment was performed with an antenna locked in place along a fixed axis, the results should be interpreted also with respect to a scanning antenna. The basis of such an interpretation would be the assumption that the effect was due to angle-of-arrival variations due to refractive bulk effects.

A theoretical analysis of antenna-to-medium coupling due to the variability of refractive effects during rain events should be

undertaken. Rain would be modeled as a medium of varying refractive index, similar to the treatment of propagation through clear-air turbulence. This model should also be used to calculate potential interference effects due to scattering by rain.

Data taken with the angle-of-arrival experiment in 1979-80 should be reexamined to determine whether the angle-of-arrival excursions observed were consistent with the antenna-degradation results obtained during the current contract period.

IX. REFERENCES

[1] D.B. Hodge and T.C. Lee, The Comstar D/3 Antenna Gain Degradation Experiment, Report 712759-5, June 1981, The Ohio State University ElectroScience Laboratory, Department of Electrical Engineering; prepared under Contract NASW-3393 for NASA.

[2] H.W. Arnold, D.C. Cox, H.H. Hoffman, "Antenna Beamwidth Independence of Measured Rain Attenuation on a 28-GHz Earth-Space Path", IEEE Trans AP-30, pp. 165-167, March, 1982.

[3] C.D. Calhoun, Jr., ATS-F Millimeter Wave Experiment Ground Receiver System for NASA-sponsored Participating Stations, Report GSFC-X-751-73-3, NASA/Goddard Space Flight Center, January 1973.

[4] V.J. Falcone, L.W. Abreu, E.P. Shettle, Atmospheric Attenuation of Millimeter Waves: Models and Computer Code, AFGL-TR-79-0253, Air Force Geophysics Laboratory, 1979.

[5] W.J. Wiscombe, "Improved Mie Scattering Algorithms", Appl. Optics, Vol. 19, No. 9 pp. 1505-1509, 1 May, 1980.

[6] CCIR Study Groups 1978-82, Doc. USSG-SF-8, Propagation Data Required for Space Telecommunication Systems, (Draft Revision of Report 564-1, Mod I), January 7, 1981.

[7] D.B. Hodge, An Improved Empirical Model for Diversity Gain on Earth-Space Propagation Paths, Report 713656-1, September 1981, The Ohio State University ElectroScience Laboratory, Department of Electrical Engineering; prepared under Contract #956013 for Jet Propulsion Laboratory, California Institute of Technology.